EPJ Web of Conferences **6**, 26002 (2010)
DOI:10.1051/epjconf/20100626002

Residual stresses in AlCrN PVD thin films

T.H.T. Pham, E. Le Bourhis, P. Goudeau and P. Guérin.

Institut P' CNRS - Université de Poitiers - ENSMA, UPR 3346, 86962 Futuroscope, France

Abstract. Residual stresses may affect the mechanical stability of high quality coatings such as $Al_{1-x}Cr_xN$. In this study, two different physical vapour deposition techniques leading to different residuals stress states have been used for depositing $Al_{1-x}Cr_xN$ coatings varying the chromium content. The structure and residual stress state have been investigated in $Al_{1-x}Cr_xN$ coatings deposited on silicon substrates using X-ray diffraction, curvature measurements and nanoindentation. The obtained results are compared to literature and commented in view of the coating microstructure.

1 Introduction

The excellent qualities such as high hardness, good abrasive, sliding wear resistance, high oxidation and corrosion resistance, of AlCrN attracted many researchers. This ternary nitride coating system protects the steel surface very efficiently from chemical attack by casting alloys and retards the formation and propagation of thermal cracks. Mechanical properties like hardness and residual stresses have been surveyed extensively (Fig. 1) with discrepancies appearing between authors [1-7]. Thin films adherent to bulk substrates are often in a state of tensile or compressive residual stress, which may affect their physical properties. In fact, residual stresses influence directly almost all properties of thin films, and thus are of great importance with respect to their usage. Stresses may be divided into three main types: epitaxial stresses, thermal stresses and intrinsic stresses [8]. Latter stresses can result from numerous transformations, such as the film densification during the deposition in the case of sputtered thin films, vacancy or interstitial diffusion, phase's transformations.

2 Experimental strategy

Two methods were employed to produce the AlCrN films. Firstly, they were deposited on the silicon (100) by NORDIKOTM3000 Elfa Systems. Two ion sources with neutraliser: Ø100mm R.F. NordikoTM, filament less, multi-target holders (4 positions), targets are 99.99% metallic Ar and Cr, the gas was N_2. This device has the advantage of high-level ion bombardments being continuously provided during the deposition process. Secondly, films were deposited on silicon (100) by System of vacuum deposits Concept™ Alliance by Pulverization Magnetron Gencoa™ 3 " (PUMA) with introduction from gas internal and walked on, at T = 300°C, targets were 99.99% metallic Al and Cr, the gases were Ar and N_2.

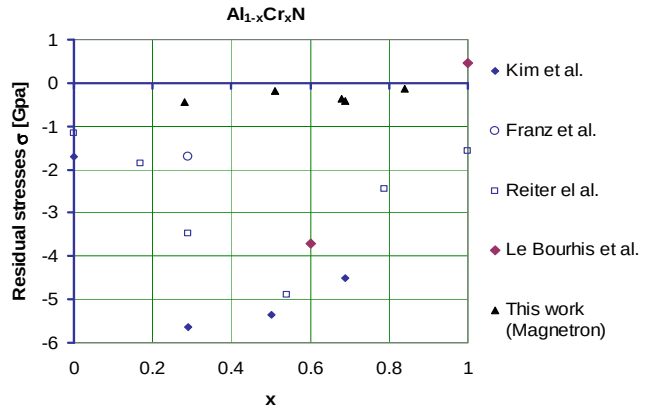

(a)

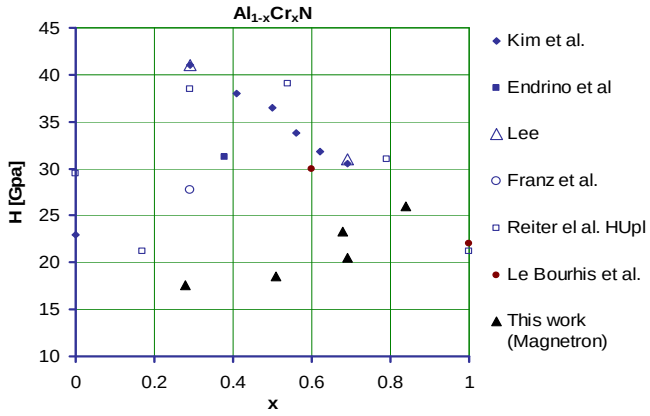

(b)

Fig. 1. Literature survey of (a) residual stresses and (b) hardness published for AlCrN thin films

Energy Dispersive X-ray Spectrometry (EDXS) JEOL- SSM- 5600LV Scanning Electron Microscopy (SEM) was used to determine the chemical compositions of films.

X-ray diffraction (XRD) measurements were conducted in the Bragg- Brentano configuration (reflection mode) on a four-circle Seifert XRD3000 diffractometer working with CuKα_1 wavelength (0.15406 nm), standard slits and a conventional punctual detector. Parameters such as peak position, width and intensity were extracted from all XRD diagrams using the EVA code from Diffract + software package (Socabim) in view of the measured diffraction diagrams available with powder diffraction files (Powder Diffraction File of the International Centre for Diffraction, PDF- ICDD).

Hardness was obtained by nano-indentation experiments at room temperature by a Berkovich diamond pyramid (using a nano-hardness tester machine from CSM -Switzerland). The tests were performed in air with the force control mode of the machine. The loading- unloading procedure was as follows: loading to maximum load in 30 s, plateau at maximum load for 30 s, unloading in 30 s. the maximum load was varied between 0.5 and 300 mN. The calibration procedure suggested by

Oliver and Pharr (1992) was used to correct the data for the load-frame compliance of the apparatus and for the imperfect shape of the indenter tip.

The macroscopic (mean) residual compressive stresses of films were determined by accurate measurement of uncoated and coated substrate profiles with a DEKTAK IIA and using Stoney's formula.

$$\sigma_{film} = \frac{E_{substrate}}{1-\nu_{substrate}} \frac{H^2}{6h} \left(\frac{1}{R_f} - \frac{1}{R_i} \right) \tag{1}$$

Where H is the substrate thickness (≈ 200 µm), h film thickness, R_f (final), R_i (initial) curvatures.

XRD method (so called $\sin^2\Psi$ method) was further used to determine the in-grain stresses σ. The in-grain residual strain measurements were performed changing the angle ψ between the normal to the surface and the normal to the diffracting planes from 0 to 55°. This can be done for the three following diffracting planes since the film is <200> textured: (111) for psi = 54.7°, (200) for psi = 0° and (220) for psi = 45°. Stresses were calculated from the strains, using the X-ray elastic constants of the diffracting phase. We employ in the following the logarithm strain usually (and correctly) approximated by the engineering strain in the elastic domain [9]. The well-known $\sin^2\psi$ equation, valid in the case of the existence of an isotropic biaxial stress state has been employed for this purpose [10-11].

$$\ln(a) = \frac{1+\nu}{E}\sigma \sin^2\psi - 2\frac{\nu}{E}\sigma + \ln(a_0) \tag{2}$$

In the above equations a and a_o are the lattice parameter for the stressed and unstressed states respectively, E and ν the elastic modulus and Poisson ratio of the diffracting phase and σ the amplitude of the residual stresses. When plotting the ln(a) as a function of $\sin^2\psi$ curves, a linear behaviour is expected and the residual stress is then deduced from the slope of the fitted linear curve while the stress free lattice parameter can be extracted from the ordinate intercept. Deviations from the linearity may be due to texture and elastic anisotropy (oscillations) and/or stress gradient effects [10].

3 Results and discussion

The study comprises a wide range of $Al_{1-x}Cr_xN$ compositions. This paper however focuses on a limited range where the overall experiments detailed above could be carried out. Preliminary results show that the structure is changing with the composition from AlN type hexagonal structure at low chromium content to CrN type cubic structure at higher Cr content. A cubic structure with a strong (200) fibber texture is then obtained for Cr compositions between 60 and 80 at%. For these coatings, Fig. 2 confirms the presence of compressive stresses for both types of deposition techniques except for thicker samples where in-grain residual stresses are tensile with weak amplitude while the global stress measured by curvature method remains the same. This can be due to microstructural changes during film growth.

Taking into account the elastic constants of bulk CrN (E=256 GPa et ν=0.3), we obtained in-grain residual stress σ and stress-free lattice parameter a_0 (Table 1). Obtained average stresses are much lower for magnetron specimens and this is to be correlated to the low hardness values that were obtained (Fig. 1). In-grain stress values are twice as large as those obtained using curvature method

for thin films fabricated by magnetron (Fig. 3a). Those stresses values cannot be compared directly, since XRD yields in–grain information while curvature method averages both crystallites and grain boundaries. However, one may note the <200> texture effects and/or the over-estimate of the elastic modulus. In fact, preliminary results from nanoindentation show that the expected Young's modulus may be much lower (about 40 %) than the one of pure CrN given in the literature and increases with Cr content up to 80 at.%. Furthermore, the system could be elastically anisotropic but the different experimental points on the $\sin^2\psi$ curves are on a straight line so if it exists it must be weak effect. Higher compressive stresses are specific to supported films elaborated by ion-beam sputtering (Fig. 3b) and can be explained by the "atomic peening" phenomenon and the incorporation of impurities, in particular Ar atoms from the sputtering gas.

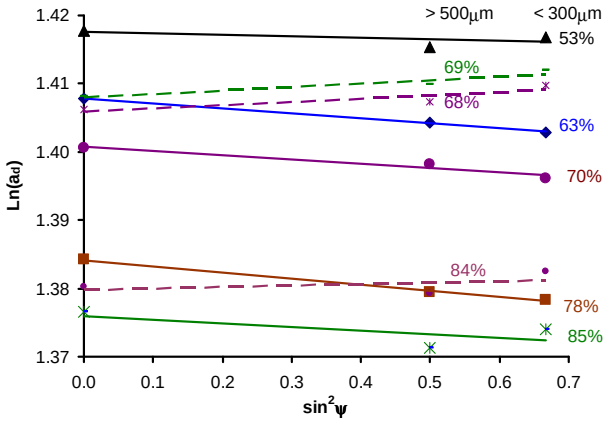

(a)

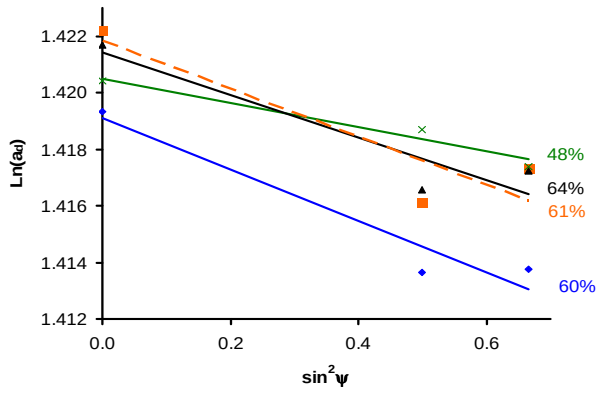

(b)

Fig. 2. $Ln(a_d)$ as a function of $\sin^2\Psi$ for AlCrN thin films obtained by (a) magnetron sputtering (PUMA) and (b) ion beam sputtering (NORDIKO).

Chromium is a high melting temperature metal. It is characterized by low atomic mobility at deposition temperature. Aluminum is a metal with relatively low melting temperature and consequently high atomic mobility at the deposition temperature. Due to materials properties, when

we increase the atomic percent of chromium atoms in the films, the residual stresses tend to decrease in both methods.

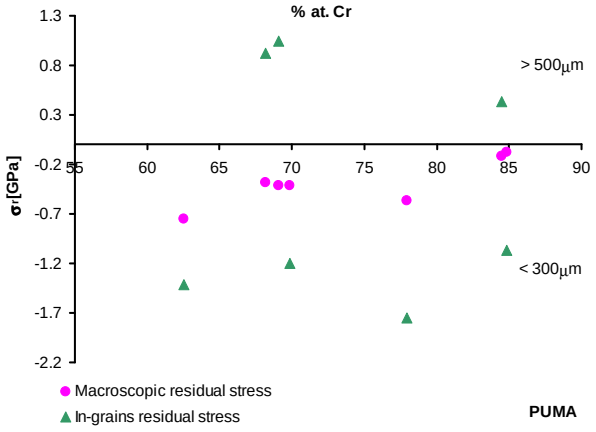

(a)

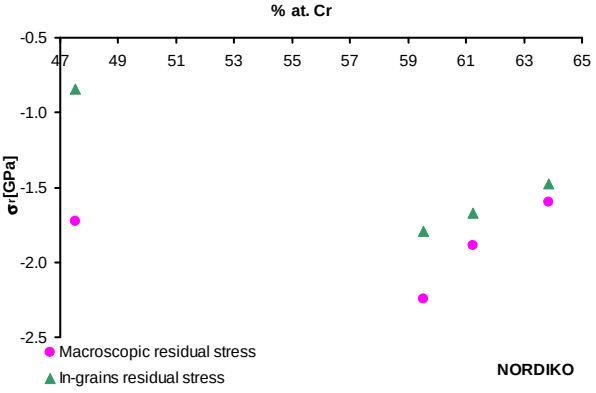

(b)

Fig. 3. Macroscopic and in-grains residual stresses values of AlCrN thin films elaborated by (a) magnetron (PUMA) and (b) ion-beam (NORDIKO) sputtering

In addition, values of stress-free lattice parameter a_0 strongly decreases from 4.13 to 3.97 A° when the atomic percent of Cr atoms increases from 53 to 85 at. % for magnetron films while a_0 for ion-beam sputtering films tends to slightly increase from 4.14 to 4.16 A° with the increase of Cr from 48 to 64 at.% (See Fig. 4). Let us recall that the lattice parameter for bulk CrN is 4.14 A°. For Nordiko samples, the presence of a large amount of interstitial defects associated with Ar atoms incorporation during the energetic ion-beam deposition may explain the lattice parameter increase. However, the strong decrease observed for Puma's samples could be correlated to the variation of nitrogen content in the samples. All these observations illustrate the strong correlation between stresses and microstructure.

Chason et al. (2002) [12] made the important observation that the compressive stress evolution was sensitive to growth rate. In particular, they observed that the steady-state compressive stress was

lower at higher growth rates. However, Fig. 5 shows that a constant growth rate was employed on most composition range and was identical for both methods.

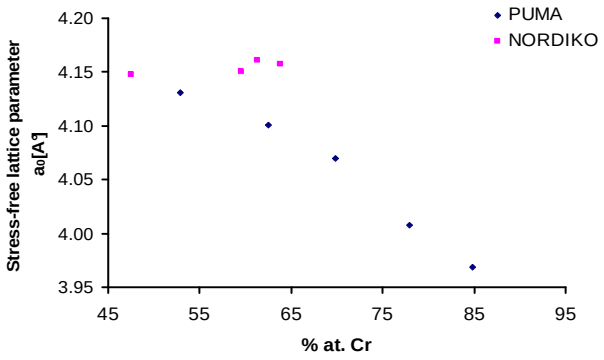

Fig. 4. Stress-free lattice parameter of AlCrN thin films elaborated by magnetron (PUMA) and ion-beam (NORDIKO) sputtering

Table 1. Chemical composition, stress-free lattice parameter, in-grain residual stress, macroscopic residual stress, of thin films AlCrN elaborated by magnetron (PUMA) and ion-beam (NORDIKO) sputtering

	% at. Cr	Slope	Intercept	Stress- free lattice parameter a_0 [A°]	In-grain residual stress σ_r [Gpa]	Macroscopic residual stress σ [Gpa]	Thickness [µm]
Puma	53	-0.0022	1.4175	4.131	-0.43	-0.62	< 300
	63	-0.0072	1.4078	4.101	-1.42	-0.75	< 300
	68	0.0047	1.4059	4.070	0.93	-0.38	> 500
	69	0.0053	1.4079	4.077	1.04	-0.41	> 500
	70	-0.0061	1.4007	4.069	-1.20	-0.41	< 300
	78	-0.0089	1.3841	4.008	-1.75	-0.57	< 300
	84	0.0022	1.3798	3.970	0.43	-0.12	> 500
	85	-0.0054	1.376	3.969	-1.06	-0.08	< 300
Nordiko	48	-0.0043	1.4205	4.147	-0.85	-1.72	< 300
	60	-0.0091	1.4191	4.151	-1.79	-2.25	< 300
	61	-0.0085	1.4219	4.161	-1.67	-1.89	< 300
	64	-0.0075	1.4214	4.157	-1.48	-1.60	< 300

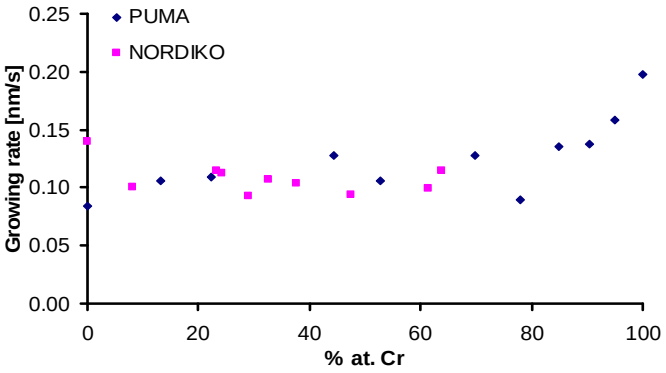

Fig. 5. Growing rate versus % at. Cr of AlCrN thin films elaborated by magnetron (PUMA) and ion-beam (NORDIKO) sputtering

4 Conclusion and perspectives

Cubic AlCrN films have been synthesized by PVD techniques. Global and in grain residual stresses were determined to be weaker for magnetron sputtering as compared to ion-beam sputtering. Residual stresses magnitude decreases with the increase of chromium content in these PVD thin films. The discrepancy between in grain stress and global stress in not yet well understood. It may be attributed to an overestimate of elastic constant used for X-ray stress calculation. Nanoindentation tests show that the Young modulus is much lower than the bulk one and increase with Cr content. However, these results must be confirmed using Brillouin scattering for example which allows precise analysis of film elasticity.

Further work includes the determination of N stoechiometry that is known to play important role and may be at the origin of the observed dispersions in the literature. Mechanical properties (Elastic modulus and tribological performance) will be surveyed.

References

1. E. Le Bourhis, P. Goudeau, M. H. Staia, E. Carrasquero, E.S. Puchi-Cabrera, Surface and Coatings Technology, **203** (2009) 2961.
2. J. L. Endrino, G.S. Rox-Rabinovich, C. Gey, Surf. Coat. Techn. **200** (2006) 6840.
3. R. Franz, J. Neidhardt, B. Sartory, R. Kaindl, R. Tessadri, P. Polcik, V.H. Derflinger, C.Mitterer, Tribology Lett. **23** (2006) 101.
4. G.S. Fox-Rabinovich, B.D. Beake, J.L. Endrino, S.C. Veldhuis, R. Parkinson, L.S. Shuster, M.S. Migranov, Surf. Coat. Techn. **200** (2006) 5738.
5. G.S. Kim, S.Y. Lee, Surf. Coat. Techn. **201** (2006) 4361.
6. S. Lee, Diff. Defect Data Pt. B: Sol. State Phenom. **124-126** (2007) 1609.
7. A.E. Reiter, V.H. Derflinger, B. Hanselmann, T. Bachmann, B. Sartory, Surf. Coat. Techn. **200** (2005) 2114.
8. Doerner, M.F. & Nix,W.D. Crit. Rev. Solid State Mater. Sci. **14**, (1988) 225-268.
9. J. Lu, Handbook of Measurement of Residual Stresses, 343 Fairmont Press, Lilburn, GA, 1996.
10. G. Maeder, Chem. Scr. **26 A** (1986) 23;
11. V. Hauk. Structural and residual stress analysis by non destructive methods: evaluation, application, assessment. Amsterdam: Elsevier; 1997.
12. E. Chason, B. W. Sheldon, L. B. Freund, Phys. Rev. Lett. **88** (2002), 156103